Journal of Lasers, Optics & Photonics
ISSN: 2469-410X

Ravindra Reddy et al., J Laser Opt Photonics 2017, 4:3
DOI: 10.4172/2469-410X.1000171

Research Article Open Access

Spectroscopic Characterization of Bentonite

Ravindra Reddy T[1], Kaneko S[2]*, Endo T[3] and Lakshmi Reddy S[1]

[1]Department of Physics, Sri Venkateswara Degree College, Kadapa, Andhra Pradesh, India
[2]Kanagawa Institute of Industrial Science and Technology, Ebina, Japan
[3]Sagamihara Surface Treatment Laboratory, Sagamihara, Japan

Abstract

A light yellow colored bentonite clay mineral obtained from India is studied. X ray diffraction (XRD) studies are suggesting that Fe_2O_3, Al_2O_3, quartz and Ca bentonite phases are present in the compound. Ca-bentonite is the major constituent and its unit cell is monoclinic with a=5.16, b=8.798, c=9.347Å and β=100.46^0. Internal structure studied using Transimission electron microscope (TEM) suggests that the clay consists of iron oxide, aluminium oxide, quartz, Ca bentonite. Tetrahedral and octahedral layers are present. Fe^{3+} is present in the location of Al^{3+} in the unit cell of Ca-bentonite. Electron paramagnetic resonance (EPR) results indicate that the unit cell of the crystal contains Fe(III), and its g values are found to be 4.19 and 2.13. IR studies are indicating that the presence of silicate and hydroxyl anions as ligands. Nonlinear optical measurements are indicating that the compound is having good potential applications in laser safety devices.

Keywords: Bentonite; XRD; TEM; EPR; Water and silicate fundamentals; Optical limiting

Introduction

Bentonite is abundant in earth's crust. It occurs in yellow, black gray, brownish color. It consists of montmorillonite as basic mineral, a sub group of smetites. In addition these it also contains other minerals, such as quartz, calcite, feldspar, gypsum, dolomite, muscovite, plagioclase, ferruginous compounds and biotite. Since it is clay, it swells when in water and it readily absorbs a wide range of metals and other minerals. Due to this reason it is used for oil drilling mud formulation, fillers for paper, pharmaceutical products, adsorbents and catalyst in the chemical process industries [1]. Also it is used in the fabrication of bricks. This clay has wide application in the pharmaceutical and plastics industries. In medical field, it finds application as a base for many dermatologic formulas [2]. Bentonite is clay because of its swelling and contracting properties destroys the root system of seedling or plants. The ideal formula of montmorillonite is $Si_{8-x}Al_x+Al_{4-y}+Mg_y(Fe)+O_{20}(OH)_4nH_2O$ where (x<y)and 0.4 <x+y<1.2. {Tetrahedral layer+octahedral layer+ interlayer cations} [3]. Depending upon the cation exchange the bentonites (montmorillonite) are classified as

(i) Sodium bentonite [$Na\ (Al, Fe,Zn)_2\ (Al,Si)_4O_{10}\ (OH)_2\ nH_2O$],

(ii) Magnesium bentonite [$Mg\ (Al, Fe,Zn)_2\ (Al,Si)_4O_{10}\ (OH)_2\ nH_2O$]

(iii) Calcium bentonite [$Ca\ (Al, Fe,Zn)_2\ (Al,Si)_4O_{10}\ (OH)_2\ nH_2O$]

(iv) Lithium bentonite [$Li\ (Al, Fe,Zn)_2\ (Al,Si)_4O_{10}\ (OH)_2\ nH_2O$].

Sodium bentonite is usually termed as bentonite, whereas calcium bentonite is called "fuller's earth". The commercial value depends on its physico-chemical properties rather than its chemical composition. Majority bentonites occurring worldwide are of the calcium type. This Ca-bentonite has lower swelling when compared to that of Na-bentonite. It is used as an adsorbent in cooking oil industries, and lubricant oil recycling, as a catalyst, adsorber, filler, etc. A major difficulty in the processing of bentonites into commercially acceptable grade is their appearance. The chemical composition as well structure of bentonite is not always same and varies from place to place. Therefore, a specific purification method for each bentonite needs to be developed depending upon the surface properties of its clay and non- clay minerals [4]. Bentonite belongs to a group of layered silicates. Literature review reveals that the chemical composition of calcium bentonite is not constant and varying with origin. Generally clays consist of Si, Al, H_2O, Fe, alkalies and alkali earths [5].

The basic structure of bentonite is composed of two atomic lattice units namely tetrahedral and octahedral layers. Tetrahedral layer contain Si^{4+} ion in the centre and surrounded O^{2-}ions. Octahedral layer consists of Al^{3+} ion in the centre and surrounded by six OH^- ions at the corners. Ion exchange of Si^{4+} and Al^{3+} with a lower valency cations such as $Fe^{3+}/Mg^{2+}/Ca^{2+}$, Na^+ take place. [6,7]. So far no spectroscopic studies are carried out on Chitradurga, Kartanataka, India bentonite, therefore the authors have undertaken to study the spectral behaviour of this caly. In the present investigation, XRD, TEM, EPR and FTIR techniques and nonlinear optics are used to know the crystalline phase and site symmetry of Fe^{3+} in the mineral.

Experimental

Yellowish colored bentonite sample originated from Chitradurga of Karnataka state, India is used in the present investigations. In order to identify the phase structure, XRD pattern of the mineral compound powder is determined by means of Philips X-ray diffractometer operated in reflection geometry at 30 mA, 40 kV with Cu-K_α (λ=1.54060 Å). The source is kept at 25°C. Data are collected using a continuous scan rate of 1° per 2 min which is then refined into 2 theta steps of 0.02°. The TEM images are obtained on Philips CM 200 transmission electron microscope operating at 200 kV having a resolution 0.23 nm. EPR spectra of the powdered sample are recorded at room temperature (RT) on JEOL JES-TE100 ESR spectrometer operating at X-band frequencies (υ=9.4446647 GHz), having a 100 KHz field modulation to obtain a

***Corresponding author:** Kaneko S, Professor, Kanagawa Institute of Industrial Science and Technology, 705-1 Shimo-Imaizumi, Ebina, Kanagawa 243-0435, Japan, Tel +81-46-236-1500; E-mail: satoru@kanagawa-iri.jp

Received November 10, 2017; **Accepted** December 04, 2017; **Published** December 20, 2017

Citation: Ravindra Reddy T, Kaneko S, Endo T, Lakshmi Reddy S (2017) Spectroscopic Characterization of Bentonite. J Laser Opt Photonics 4: 171. doi: 10.4172/2469-410X.1000171

first derivative EPR spectrum. DPPH with a g value of 2.0036 is used for g factor calculations. TEM images are obtained using Philips CM 200 transmission electron microscope operating at 200 kV having a resolution 0.23 nm. FTIR spectrum of the compound is recorded at RT on Carey 5E UV Vis-NIR spectrophotometer in powder form in the range 200-4000 cm^{-1}.

Results and Analysis

XRD

Figure 1 shows XRD spectrum of bentonite recorded on the Philips diffractometer at 25°C. Peaks are characterized using the Scherrer formula. It shows the presence of a Fe_2O_3, Al_2O_3, quartz and Ca- bentonite. Among them Ca- bentonite is a major constituent. The unit cell constants obtained from these peaks for Ca-bentonite are a=5.17 Å, b=8.798 Å and c =9.95 Å and β= 99.54^0. This result confirms that the mineral adopts a monoclinic structure. Units morphology index (MI) is developed from full width half mean (FWHM) of a peak of XRD data. The FWHM of two peaks are related with MI to its particle morphology. MI is $MI = \frac{FWHM_h}{FWHM_h + FWHM_P}$ obtained using the equation. Where $FWHM_h$ is highest FWHM value obtained from peaks and $FWHM_p$ is value of particulars peak's FWHM for which MI is to be calculated. The MI is lying in between 0.50 and 0.93. Lorentz polarization factor is the most important of the experimental quantities that control X-ray intensity with respect to diffraction angle. In the intensity calculations Lorentz factor is combined with the polarization factor and further the variation of the Lorentz's factor with the Bragg angle (θ) is shown. The overall effect of Lorentz factor is to decrease the intensity to these in the forward or backward directions. Lorentz factor $LF = \frac{\mathrm{Cos}\,\theta}{\mathrm{Sin}^2 2\theta} = \frac{1}{4\mathrm{Sin}^2\theta\cos\theta}$ using the X-ray data Lorentz polarization factor is calculated using the formula $LPF = \frac{1+\mathrm{Cos}^2 2\theta}{\mathrm{Sin}^2\theta\mathrm{Cos}\,\theta}$ [8]. The LPF is varied from 4.37 to 64.0, where LF is in between 0.95 to 8.50. The particle size of the mineral is evaluated from the line broadening of the peak (120, maximum intensity 100%) using Debye-Scherrer equation $D_{(120)} = \frac{0.9\lambda}{\beta_{1/2}\cos\theta}$ =118.7 nm. Here D is the particle size of the crystal, λ is the wavelength of incident X ray, θ is the corresponding Bragg angle, $\beta_{1/2}$ is the full width at the half maximum height (FWHM) of the peak.

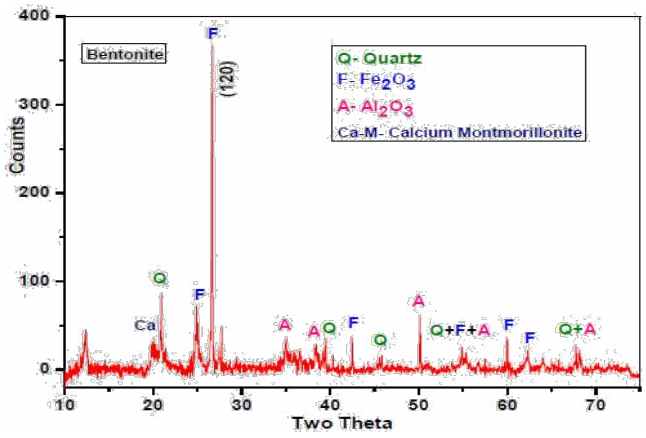

Figure 1: XRD spectrum of bentonite mineral.

TEM analysis

Bright field TEM images of bentonite are shown in Figure 2. These will help us in knowing the size, shape and to confirm the nano crystalline nature. From the Figure 2 it is noticed that the bentonite contains several clusters of different sizes and shapes. The dark spheres represent both Fe_2O_3 and Al_2O_3. The larger spheres due Fe_2O_3 and smaller spheres are due to Al_2O_3. The ionic size of Fe^{3+}(0.64Å) is large when compared to Al^{3+} (0.50 Å). Further substitutional effect of larger Fe^{3+} (0.64Å) ions, replace smaller Al^{3+} (0.50 Å) ions at octahedral site. Hence the large spheres are due to Fe_2O_3 and small spheres are due to Al_2O_3. Figure 2 shows those discontinuous layers enveloping the relatively large grains and exhibiting a typical curved lens shaped morphology with no preferred orientations. This suggests that the bentonite had well-defined polygonal growth forms with octahedral and tetrahedral shapes and other geometrical shapes. The tetrahedral and octahedral layers are arranged in the form of layers. Further the dominant mineral in the clay size fraction is mixed layers of calcium bentonite. Further it is seen that the particle size is less than 200 nm. Certain (octahedral) grains have a bigger size and some (tetrahedral) have smaller size and all of are less than 200 nm. The grain size distribution is broader and indicates the polycrystalline nature. These observations are in good agreement with reported results [9]. Layer terminations (dislocations) are common and contrast varies markedly along individual layers and between layers.

TEM analyses also indicating that the dominant mineral in the clay size fraction is Ca-bentonite. Further from the TEM images, the following are noticed as Fe_2O_3, Al_2O_3, hydroxyl, Ca etc., and are shown in Figure 2. These results are further supported by XRD results.

EPR spectral analysis

Figure 3 shows the spectrum of the powdered bentonite mineral at room temperature. It shows two resonant signals one in high field and other in low field. These can be explained by considering charge compensating vacancies in the lattice, when Fe^{3+} is substituted in place of Al^{3+}, it creates a low symmetry crystal field which is further distorted because of the strong tetragonal crystal field of Fe^{3+}ion. Hence one can expect resonances from all the three Kramers doublets | ±5/2>,| ±3/2> and | ±½>. If the lowest doublet is populated, g values are obtained ranging from 0 to 9. If the middle doublet is populated gives g is 4.30 (rhombic symmetry) and if the third doublet is populated g values are

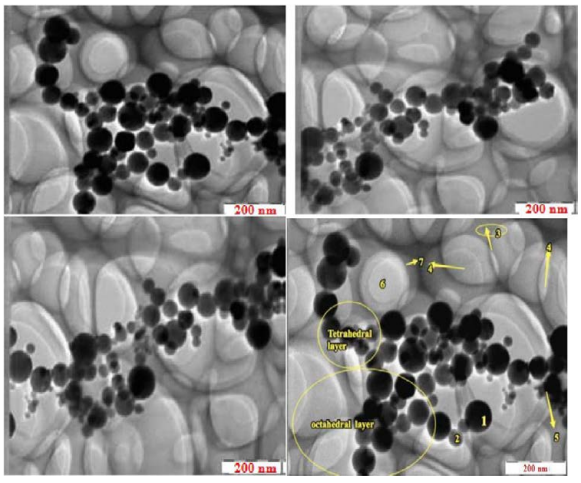

Figure 2: Different oriented TEM images of bentonite A-D i) Fe_2O_3,ii) Al_2O_3,iii) H_2O,iv) lens shaped Ca-bentonite, v)quartz, vi) Ca ,vii) Ca core.

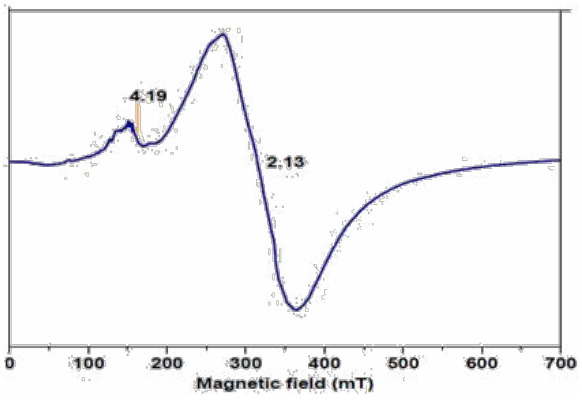

Figure 3: EPR spectrum of bentonite at RT (v=9.446647 G Hz).

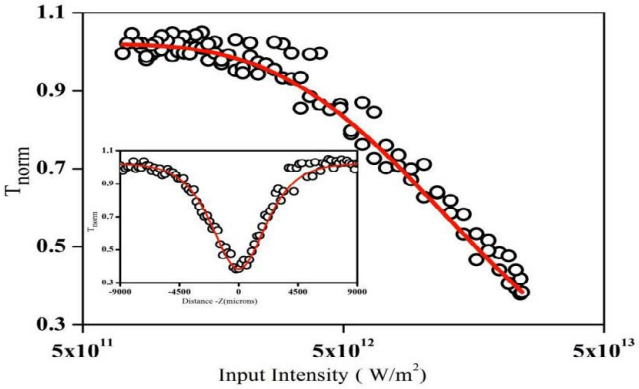

Figure 4: FTIR spectrum of bentonite.

2/7 and 30/7 [10-12]. A few systems are known which show resonances from all the three Kramers doublets. Accordingly, the EPR spectrum of the bentonite mineral shows with g values of 4.19 and 2.13 due to Fe^{3+} impurity. These results are suggesting that the majority of the bentonite clays contain more than one Fe^{3+} ion in the crystal lattice. Furthermore, this observation is also in accordance with the reported values [13].

IR Spectral analysis

The FTIR spectrum of bentonite sample recorded in the range 4000 to 400 cm^{-1} is shown in Figure 4. It shows the bands in the higher region at 3854,3753,3696,3620, 3445, 2925, 2854, 1630 and lower region at 1384, 1104, 1032, 1009, 913, 797, 695, 538, 470,433 cm^{-1}.

A very sharp multiple bands observed from 3696 to 3854 cm^{-1} are assigned to Al-OH-Al in the mineral. A single very sharp band observed at 3620 cm^{-1} followed by a broad band at 3445 cm^{-1} in the mineral is assigned to OH stretching (ν_3) of structural hydroxyl groups and water present in the mineral [14,15]. This indicates the possibility of the hydroxyl linkage between octahedral and tetrahedral layers. A very sharp and intense band observed at 1630 cm^{-1} is due to ν_2 the asymmetric OH stretch (deformation mode) of water and is a structural part of the mineral. The bands around 3700 cm^{-1} are due to hydroxyl group in di-octahedral part of the mineral each pair of Al^{3+} ions has two OH groups which are related by centre of symmetry between Al^{3+} [16,17].

FTIR spectrum of bentonite in the lower region shows bands at 1385, 1104, 1032, 1009, 913, 797, 695, 538, 470, 433 cm^{-1}. These bands are due to the vibrational modes of SiO_4 tetrahedron. The two components of maximum absorption sharp band at 1032 and 1010 cm^{-1} is a characteristic of layered silicate montmorillonite mineral and is assigned to the triply degenerate Si-O stretching ν_3 (in-plane) vibration. The band observed at 913 cm^{-1} is assigned to OH deformation mode of Al-Al-OH or Al-OH-Al. The band observed at 797 cm^{-1} corresponds to ν_1 mode. This indicates that the degeneracy is partially removed [18,19]. The band observed at 538 cm^{-1} corresponds to ν_2 the deformation mode of Al-O-Si group. The bands at 470 cm^{-1} and 433 cm^{-1} are attributed to Si-O-Si deformation band. The bands at 538, 695 and 797 cm^{-1} are attributed to ν_2, ν_4, and ν_1 modes of vibrations, respectively. These results are in agreement with reported values of bentonites obtained from other sources. Two sharp bands observed at 2925,2854 cm^{-1} are assigned to overtones and combination tones of $\nu_3+2\nu_1$ (1032+1009+913=2954 and 1032+2 x913=2858) of SiO_4. A sharp triply degenerate band at 1385 cm^{-1} (2 x 695=1390) is due to overtone of ν_4 of SiO_4.

Non-linear optics

We employed the open aperture Z-scan technique for measuring the absorptive nonlinearity of the sample. The sample solution made in DMF had a linear transmission of 74% at the excitation wavelength of 532 nm, and measurements were done for an input energy (E_{in}) of 50 μJ. In this experiment, the sample transmission is measured while it is translated by means of a linear translation stage along the axis of a focused laser beam (z-axis). By fixing E_{in} and moving the sample along the laser beam near the focal region, the incident laser fluence ($F_{in}(z)$) can be gradually varied. For a spatially Gaussian laser beam, $F_{in}(z)$ for any position z can be calculated.

From the expression, $F_{in}(z)=\frac{4\sqrt{\ln 2 E_{in}}}{\sqrt[3]{\pi\omega(z)^2}}$ (1)

Where,

$\omega(z)=\omega_0\sqrt{\left(1+\frac{z}{z_0}\right)^2}$ is the beam radius. $\mathbf{z_0=\pi\omega_0^2/}$ is known as the Rayleigh range. The fluence is a maximum at the focus (z=0), and reduces towards either side from the focal point (i.e., for z>0 and z<0). The transmitted energy depends on the input fluence, and hence, on the sample position (z), for a nonlinear material. The transmitted energy was measured using a pyro-electric energy probe (Laser probe, RJP-735). The Z-scan curve, which is a plot of the normalized transmission as a function of the sample position, is shown in the inset of Figure 5. The transmission decreases with increase in input fluence (valley in the Z-scan curve), revealing that Bentonite shows a strong nonlinear absorptive property. Figure 5 shows the normalized transmission of the sample plotted against the input intensity, which is given by $\mathbf{F_{in}(z)/t}$, where **t** is the laser pulse width. The plots in Figure 5 can be numerically fitted to the relevant nonlinear transmission equation to calculate the nonlinear parameters. We found that the best numerical fit to the present data can be obtained for a mechanism consisting of two-photon absorption (2PA) and weak saturable absorption (SA) [20,21]. The corresponding nonlinear

$$\alpha(I)=\frac{\alpha_0}{1+(I/I_S)}+\beta I \quad (2)$$

where β is the two-photon absorption coefficient, and I_s is the saturation intensity. α is the unsaturated linear absorption coefficient of the sample. The corresponding

$$\frac{dI}{dz'}=\left[\frac{\alpha_0}{1+(I/I_S}+\beta I\right]I \quad (3)$$

where z' is distance of propagation within the sample. By fitting the

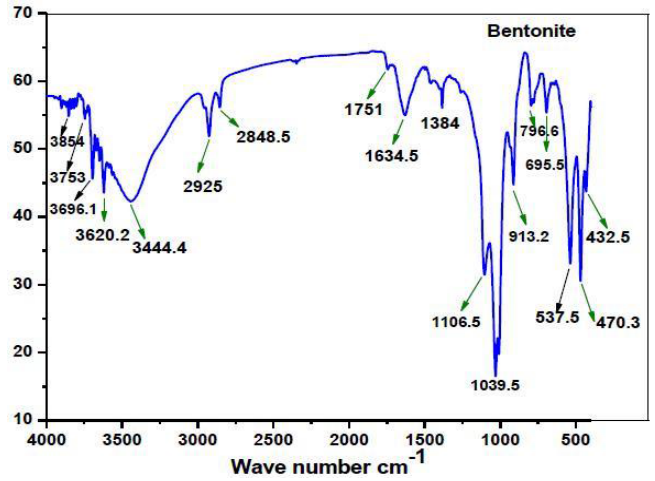

Figure 5: Nonlinear optical transmission of a DMF solution of bentonite mineral, measured by the Z-scan technique. Inset shows the Z-scan curve. Circles are data points while solid curves are numerical fits to the data.

measured data to the above equations, best-fit values of I_s=1.7 × 10 ^{12} W/m^2 and β=1.0 × 10 $^{-10}$ m/W have been obtained. These values indicate that bentonite has substantial absorptive optical nonlinearity. In the present case excited state absorption (ESA) has a strong contribution to b compared to that of genuine two-photon absorption, and therefore, b represents the combined nonlinearity of TPA and ESA.

Conclusions

The following conclusions are made from the foregoing results and analysis:

1. The chemical composition of bentonite is variable from origin.

2. XRD investigation shows that the bentonite sample contains Ca, K-, Na- and the Mg-montmorillonites minerals. Among them calcium type being the dominant mineral.

3. TEM results are suggesting that the clay contains iron oxide, aluminium oxide and Ca-bentonite as major constituents. Further the clay is formed with layered structure in which octahedral and tetrahedral units are linked through hydroxyl groups.

4. EPR spectrum is due to Fe (III) which is in a distorted octahedral environment.

5. IR spectrum of the compound indicates that water and silicate are present in the compound. Further those tetrahedral and octahedral layers are linked through hydroxyl units.

6. The strong nonlinearity observed in bentonite can have potential applications in the fabrication of optical limiters which can be employed for protecting sensitive optical detectors and human eyes from laser radiation.

References

1. Ahmad AS, Salahudeen N, jinomoh CSA, Hamza H, Ohikere (2012) A Studies on the mineral and Chemical characterization of pindiga bentonitic clay. PetroTech Develop J 1:1-8.
2. http://oregonstate.edu/.
3. www.skb.se.
4. Manocha S, Patel N, Manocha LM, (2008) Development and Characterisation of Nanoclays from Indian Clays. Defence Sci J 58: 517-524.
5. Ralph E Grim (1968) Clay Mineralogy. McGraw Hill Book Co, New York.
6. Petrović Z, Dugić P, Aleksić V, Begić S, Sadadinović J et al. (2014) Composition, structure and textural characteristics of domestic acid activated bentonite. Contemporary Materials 1: 133-139.
7. Nayak PS, Singh BK (2007) Instrumental characterization of clay by XRF, XRD and FTIR. Bull Mater Sci 30: 235-238.
8. Surayanarayana C, Grant Norton M (1998) X-Ray diffraction: a Practical Approach. Plenum Publishing Corporation New York, USA.
9. Gejing R L, Peacor D, Douglas C (1997) Transformation of smetite to illite in bentonite and associated sediment from Kaka point, New Zealand: contrast in rate and mechanism. Clays and Clay Minerals 45: 54-67.
10. Rao PS, Subramanian S (1985) Single Crystal E.P.R. Studies of Some First-Row Transition Ions in Hexaimidazole Zinc (II) Dichloride Tetrahydrate. Mol Phys 54: 415.
11. Castner T, Niawell GS, Holton WC, Slichter CP, (1960) J Chem Phys 32: 668.
12. Holmes OG, McClure DS (1957) J Chem Phys 26: 1686.
13. Craciun C, Meghea A (1985) Electron spin resonance studies of montmorillonites. Clay Minerals 20: 281-290.
14. Herzberg G (1962) Molecular Spectra and Molecular Structure. Van No strand, New York, 2: 167.
15. Hunt GR, Salisbury JW, (1970) Visible and Near-Infrared Spectra of Minerals and Rocks—I. Silicate Minerals. Modern Geology 1: 283.
16. Famer VC, Russel JD, (1964) The Infrared Spectra of Layered Silicates. Spectrochimica Acta. Spectro Chim Acta 20: 1149-1173.
17. Rotenberg B (2014) Water in clay nanopores. MRS Bulletin 39: 1074-1081.
18. Marel HWVD, Beutelspacher H (1976) Atlas of infrared spectroscopy of clay minerals and their admixtures. Els Sci Pub, Amsterdam.
19. Gupta A, Amitabh V, Kumari B, Mishra B (2013) FTIR and XRPD studies for the mineralogical composition of Jharkhand bentonite. Res J Pharma, Bio Chem Sci 4: 360-368.
20. Ann Mary KA, Unnikrishnan NV, Reji Philip (2013) ultrafast optical nonlinearity in nanostructured selenium allotropes. Chem Phys Lett. 588: 136-140.
21. Anand B, Ntim SA, Sai Muthukumar V, Sivankara Sai S, Philip R, (2011) Improved optical limiting in dispersible carbon Nanotubes and their metal oxide hybrids. Carbon 49: 4767-4773.